JACS
JOURNAL OF THE AMERICAN CHEMICAL SOCIETY
pubs.acs.org/JACS
Article

Adsorption-Induced Active Vanadium Species Facilitate Excellent Performance in Low-Temperature Catalytic NO_x Abatement

Zhihua Lian, Jie Wei, Wenpo Shan, Yunbo Yu, Petar M. Radjenovic, Hua Zhang, Guangzhi He, Fudong Liu, Jian-Feng Li,* Zhong-Qun Tian, and Hong He*

Cite This: J. Am. Chem. Soc. 2021, 143, 10454−10461

Read Online

ACCESS | Metrics & More | Article Recommendations | Supporting Information

ABSTRACT: Vanadia-based catalysts have been widely used for catalyzing various reactions, including their long-standing application in the deNO$_x$ process. It has been commonly considered that various vanadium species dispersed on supports with a large surface area act as the catalytically active sites. However, the role of crystalline V_2O_5 in selective catalytic reduction of NO$_x$ with NH_3 (NH_3-SCR) remains unclear. In this study, a catalyst with low vanadia loading was synthesized, in which crystalline V_2O_5 was deposited on a TiO_2 support that had been pretreated at a high temperature. Surprisingly, the catalyst, which had a large amount of crystalline V_2O_5, showed excellent low-temperature NH_3-SCR activity. For the first time, crystalline V_2O_5 on low-vanadium-loading catalysts was found to be transformed to polymeric vanadyl species by the adsorption of NH_3. The generated active polymeric vanadyl species played a crucial role in NH_3-SCR, leading to remarkably enhanced catalytic performance at low temperatures. This new finding provides a fundamental understanding of the metal oxide-catalyzed chemical reaction and has important implications for the development and commercial applications of NH_3-SCR catalysts.

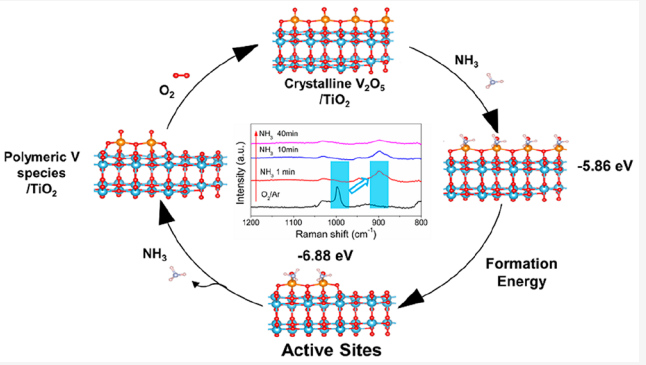

INTRODUCTION

Reactive sites are essential in heterogeneous and homogeneous catalysis. Identification and characterization of active species is a prerequisite for understanding any catalytic reaction mechanism and for the rational design of high-performance catalysts.[1] However, the species identified by common *ex situ* methods can differ from those present under realistic catalytic reaction conditions.[2−4] Therefore, it is crucial to accurately determine the active species under reaction conditions. In a number of cases, catalytic surfaces have been found to undergo reconstruction under reaction conditions.[5,6] For example, the composition and chemical state of core−shell $Rh_{0.5}Pd_{0.5}$ bimetallic nanoparticles were found to change dramatically under redox conditions.[7] Under selective catalytic reduction reaction conditions for NO$_x$ by NH_3 (NH_3-SCR), mobilized Cu ions were reported to travel through zeolite windows and form transient ion pairs that participated in an O_2-mediated $Cu^I \rightarrow Cu^{II}$ redox step integral to the catalytic reaction.[8]

Vanadia-based catalysts are attracting great interest in many industrially important processes, such as the production of sulfuric acid by SO_2 oxidation, selective oxidation of hydrocarbons, and NH_3-SCR.[9,10] NH_3-SCR of NO$_x$ over vanadia-based catalysts is a widely used strategy for controlling NO$_x$ emissions.[11−18] Vanadium species act as the active sites in the catalytic reaction. Therefore, it is important to investigate these species in depth, especially under reaction conditions.

A number of different vanadium species, such as monomeric vanadyl, polymeric vanadate, and V_2O_5 crystallites, can exist on the surface of vanadia-based catalysts used in NH_3-SCR reactions.[19,20] At low vanadia concentrations, monomeric vanadyl species can form on the catalyst surface, while at higher concentrations, polymeric vanadate species and crystalline V_2O_5 can exist on the catalyst surface.[21] Previously, we found that monomeric vanadyl species possessed lower NH_3-SCR activity than polymeric vanadyl species, especially at low temperatures.[22] The coupling effect of the polymeric structure shortened the reaction pathway for the regeneration of redox sites and substantially reduced the overall reaction barrier of the catalytic cycle. Thus, the concentration of polymeric vanadyl surface species can dictate the low-temperature activity of vanadia-based catalysts for NH_3-SCR. Surface-dispersed vanadia species have received a lot of

Received: May 27, 2021
Published: July 1, 2021

Downloaded via INST OF URBAN ENVIRONMENT on July 14, 2021 at 09:25:38 (UTC).
See https://pubs.acs.org/sharingguidelines for options on how to legitimately share published articles.

© 2021 American Chemical Society

https://doi.org/10.1021/jacs.1c05354
J. Am. Chem. Soc. 2021, 143, 10454−10461

attention, while only scant attention has been paid to crystalline V_2O_5. Crystalline V_2O_5 has usually been found to exist on catalysts with a low specific surface area or after high-temperature treatment. However, the role of crystalline V_2O_5 in the NH_3-SCR of NO_x remains unclear. Investigating crystalline V_2O_5 on catalysts in depth is beneficial to gain an understanding of the vanadia-based catalysts to enable the development of excellent NH_3-SCR catalysts.

Herein, a high-temperature (850 °C) calcination pretreatment step was used to obtain TiO_2 with a small specific surface area, on which crystalline V_2O_5 was deposited (V/Ti-850). Surprisingly, V/Ti-850 had much higher NH_3-SCR activity than the untreated catalyst (V/Ti). To further investigate the effect of pretreatment, *in situ* Raman spectroscopy was performed under real NH_3-SCR conditions. The *in situ* Raman results demonstrated that crystalline V_2O_5 in V/Ti-850 could transform to polymeric vanadyl species during NH_3 adsorption, which remarkably enhanced the catalytic performance for low-temperature NH_3-SCR of NO_x. This novel finding provides fundamental insight into the NH_3-SCR reaction and has important implications for the development and commercial application of NH_3-SCR catalysts, especially vanadia-based catalysts with low loading.

EXPERIMENTAL SECTION

Catalyst Preparation. The V/Ti catalyst was prepared by a conventional impregnation method with TiO_2 (DT-51, Millennium Chemicals) as the support and ammonium metavanadate (1.0 wt % V_2O_5) as the precursor. First, ammonium metavanadate was dissolved in oxalic acid solution followed by mixing with TiO_2 powder. Then, the resulting slurry was dried in a rotary evaporator after stirring. Finally, the obtained powder was dried overnight at 100 °C and subsequently calcined at 500 °C for 4 h in static air. TiO_2 was calcined at 850 °C for 2 h in static air to obtain Ti-850, and V/Ti-850 was synthesized with Ti-850 as a support by the same procedure used for V/Ti.

Activity Test. The activity tests were carried out in a fixed-bed quartz flow reactor with 0.3 mL of the catalyst (40−60 mesh). The reaction gas consisted of 500 ppm of NO, 500 ppm of NH_3, 5% O_2, 5% H_2O (when used), and 100 ppm of SO_2 (when used), balanced with N_2. The total flow rate was 500 mL min^{-1}, with a gas hourly space velocity (GHSV) of 100 000 h^{-1}. The concentrations of NO, NO_2, N_2O, and NH_3 were continuously analyzed by a Fourier transform infrared gas analyzer (Thermo Fisher IGS) equipped with a 2 m gas cell.

Catalyst Characterization. Brunauer−Emmett−Teller (BET) analysis, X-ray diffraction (XRD), and H_2 temperature-programmed reduction (H_2-TPR) were conducted using the procedures reported in our previous works.[22,23] The Raman spectra were measured on a Jobin-Yvon Horiba Xplora confocal Raman system. The excitation wavelength was 638 nm, and a 50× microscope objective with a numerical aperture of 0.55 was used in all Raman measurements. The laser power was controlled at about 1.5 mW. *In situ* experiments were performed in a customized Raman cell made in-house with atmospheric and temperature control. Before the Raman experiments, the samples were pretreated under O_2/Ar flow at 350 °C for 0.5 h. A reactant mixture (50 mL min^{-1}) of 500 ppm of NH_3 and/or 500 ppm of NO and 5% O_2 balanced with Ar was subsequently introduced into the *in situ* cell, and time-dependent *in situ* Raman spectra were obtained. Transmission electron microscopy (TEM) images were obtained on a FEI Tecnai G2 F20 microscope with an acceleration voltage of 200 kV. *In situ* diffuse reflectance infrared Fourier transform spectroscopy (DRIFTS) experiments were performed on a Fourier transform infrared (FTIR) spectrometer (Nicolet iS50) equipped with a Smart Collector and a MCT/A detector cooled by liquid N_2. First, the sample was pretreated in a 20 vol % O_2/N_2 flow at 300 °C for 0.5 h and then cooled to 175 °C. The background spectra were collected in flowing N_2 and automatically subtracted from the sample spectrum. The reaction conditions were controlled as follows: 500 ppm of NH_3 or 500 ppm of NO + 5 vol % O_2, 300 mL min^{-1} total flow rate, and N_2 balance. All spectra were recorded by accumulating 100 scans with a resolution of 4 cm^{-1}.

Density Functional Theory (DFT) Calculations. DFT calculations with periodic boundary conditions (PBCs) were performed using the Perdew−Burke−Ernzerhof (PBE) functional,[24] as implemented in the Vienna *ab initio* simulation package (VASP 5.4.4).[25] The projector augmented wave (PAW) method was used to describe the core−valence electron interaction.[26] All calculations were spin-polarized. The DFT+U approach was applied to the V atom in VO_x and Ti atom in TiO_2 with the values of U_{eff} = 2.0 and 2.3 eV, respectively, to describe the on-site Coulomb interactions.[27] The plane wave energy cutoff was set to 400 eV for all atoms. To calculate the formation energy of monomeric, dimeric, and crystalline V_2O_5 on TiO_2 surfaces, a (2 × 4) supercell of the anatase (101) surface with two stoichiometric TiO_2 layers was used as the substrate.[22] Atoms in the bottom stoichiometric TiO_2 layer were kept frozen at their bulk positions, whereas all other atoms were fully relaxed. Only the Γ point of the Brillouin zone was sampled. A vacuum spacing of 15 Å was used to avoid the periodic image interaction normal to the surface. The conjugate gradient algorithm was used for geometric optimization until the forces on all relaxed atoms were less than 0.02 eV $Å^{-1}$. The Gaussian smearing method with a smearing width of 0.05 eV was applied to accelerate the convergence of integration at the Brillouin zone.

RESULTS AND DISCUSSION

Structural Properties. TiO_2 calcined at 850 °C was used to support V_2O_5 (1 wt %), giving a V/Ti-850 catalyst. For comparison, a V/Ti catalyst without TiO_2 pretreatment was also obtained. As shown in Table 1, the specific surface areas of

Table 1. N_2 Physisorption Results for the Vanadia-Based Catalysts

catalyst	specific surface area (m^2 g^{-1})	average pore diameter (nm)	pore volume (mL g^{-1})
V/Ti	83.1	15.0	0.42
V/Ti-850	11.2	32.5	0.09

V/Ti and V/Ti-850 were 83.1 and 11.2 m^2 g^{-1}, respectively. TiO_2 calcination resulted in a remarkable decrease in the specific surface area and pore volume, while the average pore diameter increased. From the XRD patterns in Figure S1 of the Supporting Information, both V/Ti and V/Ti-850 possessed the crystalline anatase TiO_2 structure. However, V/Ti-850 had higher TiO_2 crystallinity as a result of the calcination pretreatment. Also, no diffraction peaks from vanadium species were observed for either of these catalysts.

Existence of Crystalline V_2O_5. The morphologies of the two vanadia-based catalysts were investigated with high-resolution transmission electron microscopy (HRTEM). In Figure 1a, it can be seen that the V/Ti catalyst had a nanoparticle-like morphology with ∼30 nm average nanoparticle diameter. In Figure 1b, the lattice fringes with 0.35 nm interplanar spacings were attributed to TiO_2 (101). No structural features of vanadium species were observed, indicating that they were highly dispersed across the V/Ti catalyst surface.

In contrast, as seen in Figure 1c, V/Ti-850 was composed of irregular particles with varying diameters between 30 and 60 nm. Besides TiO_2 (101), Figure 1d also shows lattice fringes of V_2O_5 (002), with 0.22 nm interplanar spacings. These spacings corresponded to the ∼3−5 nm V_2O_5 nanoparticles dispersed

https://doi.org/10.1021/jacs.1c05354
J. Am. Chem. Soc. 2021, 143, 10454−10461

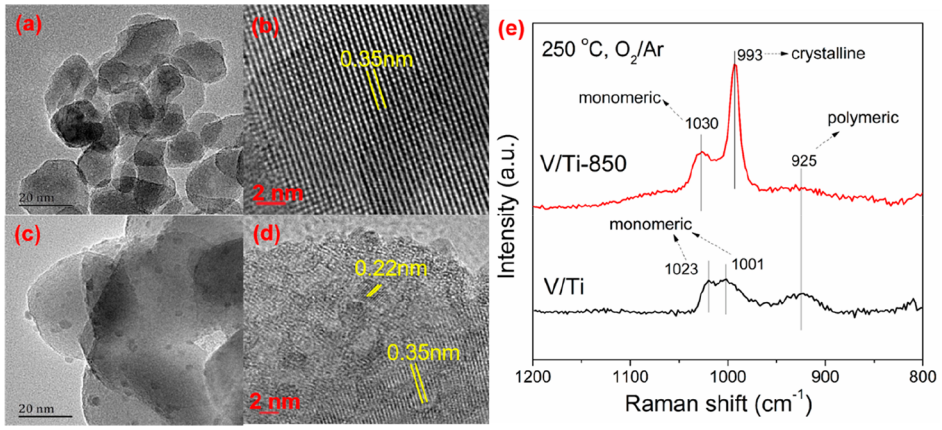

Figure 1. HRTEM images of (a and b) V/Ti and (c and d) V/Ti-850 and (e) Raman spectra of vanadia-based catalysts with (red line) and without (black line) an 850 °C calcination pretreatment step, recorded under exposure to O_2/Ar at 250 °C.

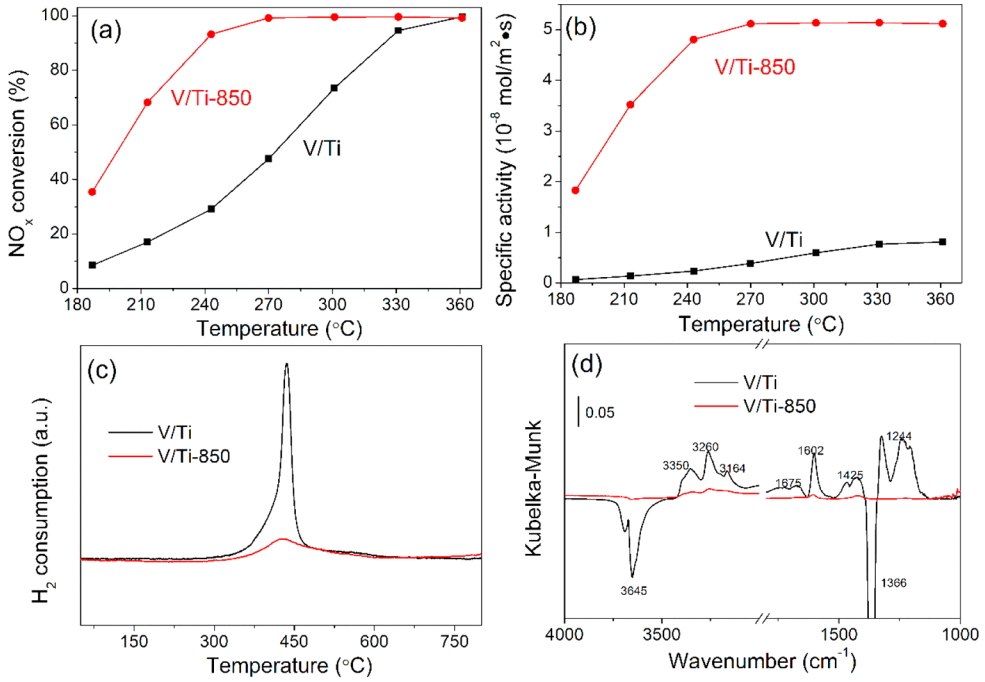

Figure 2. (a) NH_3-SCR of NO_x activity. (b) Specific activity normalized by the specific surface area over V/Ti and V/Ti-850. Reaction conditions: 500 ppm of NO, 500 ppm of NH_3, 5 vol % O_2, total gas flow rate of 500 mL min^{-1}, and space velocity of 100 000 h^{-1}. (c) H_2-TPR results. (d) DRIFTS of NH_3 adsorption over V/Ti and V/Ti-850.

on the TiO_2 support visible in Figure 1c. Thus, the 850 °C pretreatment step produced larger and more irregular TiO_2 particles and decreased the specific surface area considerably, although the anatase structure was maintained. Although crystalline V_2O_5 was observed on V/Ti-850 with HRTEM, crystalline V_2O_5 was not detected by XRD, which is likely due to the size and concentration of V_2O_5 particles being lower than the detection limit.

Raman spectroscopy was used to determine the structure of the surface vanadium species in both catalysts exposed to O_2/Ar at 250 °C, and the results are shown in Figure 1e. According to the literature,[21,28,29] the Raman bands at 1023 (1030) and 993 cm^{-1} are characteristic of monomeric vanadyl species and crystalline V_2O_5, respectively, while the band at 925 cm^{-1} for V/Ti is attributed to polymeric vanadyl species.[22] The 1001 cm^{-1} band was ascribed to vanadyl species in close proximity but still monomeric in nature.[28] In comparison to V/Ti, V/Ti-850 contained a considerably greater amount of crystalline V_2O_5 species. In combination of HRTEM and Raman, it can be concluded that abundant crystalline V_2O_5 was present on V/Ti-850, while almost no crystalline V_2O_5 was present on V/Ti. The small specific surface area of the support was the reason for the formation of crystalline V_2O_5 on V/Ti-850.

NH_3-SCR Activity. As shown above, both polymeric and monomeric vanadyl species were detected on V/Ti, while monomeric vanadyl and crystalline V_2O_5 predominated on V/Ti-850. In general, it has been recognized that surface-dispersed vanadia species are the active sites for the NH_3-SCR reaction; therefore, the formation of crystalline V_2O_5 is considered undesirable. In previous work, we showed that polymeric vanadyl species had higher activity than monomeric vanadyl species in the NH_3-SCR of NO_x.[22] Also, here, the specific surface area of V/Ti was much larger than that of V/

https://doi.org/10.1021/jacs.1c05354
J. Am. Chem. Soc. 2021, 143, 10454−10461

Ti-850. Therefore, it was expected that the SCR activity over V/Ti should be higher than that over V/Ti-850.

Thus, the NH_3-SCR activity over V/Ti and V/Ti-850 was investigated, and the results are shown in Figure 2a. NO_x conversion over V/Ti increased with the temperature, with over 90% NO_x conversion achieved above 330 °C. Surprisingly, for the V/Ti-850 catalyst, the performance was significantly enhanced, with nearly 100% NO_x conversion at 243 °C and above. More remarkably, in Figure 2b, the specific activity (activity normalized by the specific surface area) of V/Ti-850 was much higher than that of V/Ti. Even in the presence of 5% H_2O, V/Ti-850 still showed much higher NO_x conversion than V/Ti (Figure S2 of the Supporting Information). The NO_x conversion under the conditions of heating from 100 to 350 °C at the rate of 10 °C min^{-1} (Figure S3 of the Supporting Information) also exhibited that the low-temperature activity over V/Ti-850 was better than that over V/Ti. Figure S4 of the Supporting Information shows that, like 1 V/Ti, the thermal treatment of the support also improved the SCR activity of 0.5 V/Ti. However, it decreased the NO_x conversion of 3 V/Ti, indicating that the thermal treatment mainly promoted the catalytic activity of low-loaded vanadia catalysts. As a result of the existence of sulfurous compounds in fossil fuels, the effect of SO_2 on the catalytic activity of V/Ti-850 at 300 °C was also investigated (Figure S5 of the Supporting Information). The NO_x conversion of V/Ti-850 was constant at ~90% when exposed to a gas stream with 5% H_2O and 100 ppm of SO_2 for 12 h, indicating that the V/Ti-850 catalyst has excellent resistance to poisoning. This result, surprisingly, illustrates that V/Ti-850, containing abundant crystalline V_2O_5, has better catalytic performance than V/Ti, containing greater amounts of polymeric vanadyl species.

Redox Capability and Acidity. Both redox sites and acid sites are essential for the NH_3-SCR reaction and can affect the catalytic performance.[30] Therefore, the redox capability and acidity of the vanadia-based catalysts were investigated. Figure 2c shows the H_2-TPR results for the vanadia-based catalysts. Both catalysts presented a broad reduction peak centered at 430 °C, attributed to the reduction of surface vanadium or titanium species.[31,32] However, V/Ti-850 had a much lower H_2 consumption than V/Ti, indicating that it contained a lower amount of reducible species. In comparison to V/Ti-850, a stronger interaction between vanadium and titanium on V/Ti resulted in more facile reduction of titanium species, consuming a larger amount of H_2.

Next, DRIFTS was used to investigate the presence of acid sites on the vanadia-based catalysts. Figure 2d shows the DRIFT spectra acquired after exposing V/Ti and V/Ti-850 to NH_3 and purging with N_2 at 200 °C. NH_4^+ adsorbed on Brønsted acid sites (1675 and 1425 cm^{-1}) and NH_3 coordinated to Lewis acid sites (1602, 1244, 3350, and 3260 cm^{-1} and ν(N−H) of 3164 cm^{-1}) were observed.[33−35] From the spectra, the number of acid sites on V/Ti-850 was significantly lower than that on V/Ti, which should be related to the decreased specific surface area of V/Ti-850, in accordance with the NH_3-TPD results (Figure S6 of the Supporting Information). When NO_x was introduced to V/Ti and V/Ti-850 samples with pre-adsorbed NH_3, the peaks attributed to adsorbed NH_3 species gradually diminished (Figure S7 of the Supporting Information). This indicates that the adsorbed NH_3 species participate in NH_3-SCR of NO_x.

Generally, a larger specific surface area signifies more active sites, contributing to better catalytic performance. However, V/Ti-850 had a much smaller specific surface area but higher NO_x conversion than V/Ti. Surprisingly, the V/Ti-850 catalyst did not exhibit any advantages in terms of redox capability or surface acidity, of which each has been considered to be a requirement for promoting the NH_3-SCR reaction. Therefore, there must be some other factor(s) to account for the excellent catalytic performance of V/Ti-850.

Transformation of Surface Species on Catalysts. Previous reports have shown that bulk metal oxides can spread on the surface of oxide supports and that spreading of V_2O_5 over the TiO_2 surface is favored on well-defined anatase crystal planes under oxidizing conditions.[36] At 230 °C under methanol oxidation conditions, crystalline V_2O_5 completely transformed into surface vanadia species, which increased the catalytic activity.[37] To our knowledge, the spreading of vanadia during the NH_3-SCR reaction has not been reported before. We considered whether crystalline V_2O_5 species on V/Ti-850 could transform to surface vanadia species under heating or NH_3-SCR conditions.

Figure 5 shows the Raman spectra of V/Ti and V/Ti-850 under an O_2/Ar atmosphere at different temperatures. At relatively low temperatures of 30−50 °C, Raman bands at 940 cm^{-1}, attributed to polymeric vanadyl species, were observed on V/Ti (Figure 3a). With an increasing temperature, the

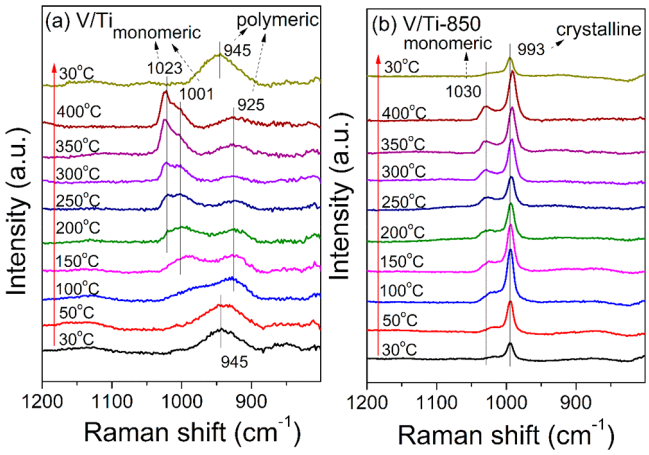

Figure 3. Raman spectra of (a) V/Ti and (b) V/Ti-850 under an O_2/Ar atmosphere at different temperatures.

bands at 1001 and 1023 cm^{-1} ascribed to surface monomeric vanadyl species appeared, and their intensity increased with a concomitant decrease in the intensity of the 940 cm^{-1} band, which also red shifted to 925 cm^{-1}. This red shift might be due to a change in the degree of polymerization of the vanadyl species.[21,29] At 400 °C, the intensity of the 940 cm^{-1} band was much weaker than at 30 °C, while the 1023 cm^{-1} band became dominant, indicating that most of the polymeric vanadyl species were transformed into surface monomeric vanadyl species. This might be the main reason for the low catalytic activity over V/Ti. It has been reported that surface migration or diffusion of vanadium species on TiO_2 occurs at temperatures high enough to overcome the intrinsic resistance.[37] Decreasing the temperature back to 30 °C caused polymerization of monomeric vanadyl species, and thus, the band corresponding to polymeric species reappeared at 940 cm^{-1}. Therefore, the vanadium species on the V/Ti catalyst can be reversibly transformed by altering the temperature.

https://doi.org/10.1021/jacs.1c05354
J. Am. Chem. Soc. 2021, 143, 10454−10461

In contrast, the vanadium species observed on V/Ti-850 behaved differently at an elevated temperature from those on V/Ti (Figure 3b). At 30 °C, two bands at 993 and 1030 cm^{-1}, attributed to crystalline V_2O_5 and monomeric vanadyl species, respectively, were observed for V/Ti-850. With an increasing temperature, the intensities of bands at 1030 and 993 cm^{-1} became stronger as a result of the higher crystallinity at a higher temperature, and no polymeric species were observed during the whole process. This phenomenon was different from the studies[36,37] that reported the thermal spreading of crystalline V_2O_5 on an oxide support surface. Decreasing the temperature back to 30 °C caused the Raman spectrum to recover to its original profile.

In situ Raman experiments were conducted to further investigate the effects of NH_3 and/or NO + O_2 on the surface structure of V/Ti and V/Ti-850. Figure S8 of the Supporting Information shows *in situ* Raman spectra of V/Ti exposed to NH_3, NH_3 + NO + O_2, and NO + O_2 atmospheres in sequence at 250 °C. The bands at 1023, 1001, and 925 cm^{-1} were visible under O_2/Ar. Upon exposure to NH_3, the bands associated with vanadium species all gradually diminished. After NO + O_2 was also introduced, the weak bands at 1001 and 925 cm^{-1} reappeared. After shutting off NH_3, the band at 1023 cm^{-1} was also observed. For the V/Ti catalyst, these results suggest that NH_3 adsorbs on monomeric and polymeric vanadyl species and then reacts with NO + O_2.

For V/Ti-850 under O_2/Ar conditions (Figure 4a), crystalline V_2O_5 (993 cm^{-1}) and monomeric vanadyl species

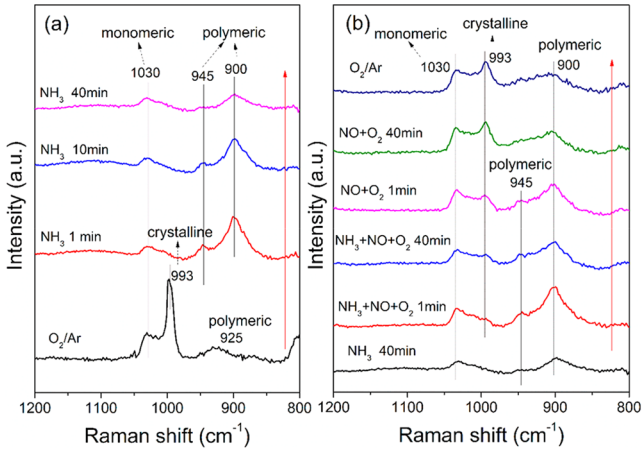

Figure 4. *In situ* Raman spectra of V/Ti-850 (a) at different NH_3 exposure times and (b) under different reaction conditions at 250 °C.

(1030 cm^{-1}) were present. Notably, upon exposure to NH_3, the band at 993 cm^{-1} disappeared and two new bands at 900 and 945 cm^{-1}, assigned to polymeric vanadyl species,[29] instantly appeared. This demonstrates that crystalline V_2O_5 completely transformed to surface polymeric vanadyl species during NH_3 adsorption. According to DFT calculations (Table S1 and Figure S9 of the Supporting Information), the formation energy was −6.00, −6.88, and −5.86 eV for NH_3-adsorbed monomeric, polymeric, and crystalline V_2O_5 on TiO_2, respectively, indicating that adsorption of NH_3 was beneficial to the formation of polymeric vanadia on TiO_2. Thus, when NH_3 was introduced, crystalline V_2O_5 transformed into polymeric vanadyl species, and these surface-dispersed vanadia species could act as active sites in the NH_3-SCR reaction, with polymeric vanadyl species being more active than monomeric vanadyl species.[19,22] Therefore, the spreading of crystalline V_2O_5 on the catalyst surface could facilitate the NH_3-SCR reaction and explains why V/Ti-850 exhibits excellent catalytic performance at low temperatures. Introducing NH_3 also caused the band at 1030 cm^{-1} to decrease, indicating that NH_3 was also adsorbed on monomeric vanadyl species.

In addition to panels a and b of Figure 4, the changes in various vanadium species on V/Ti-850 under different atmospheres, as reflected by changes in the integrated area of their Raman peaks (1030, 900, and 993 cm^{-1} for monomeric, polymeric vanadyl, and crystalline V_2O_5 species, respectively), are shown in Figure S10 of the Supporting Information. When NH_3 was introduced, the peak intensities of monomeric vanadyl and crystalline V_2O_5 both decreased, while that of polymeric vanadyl species increased immediately. With increasing the NH_3 exposure time, the intensity of the 900 cm^{-1} band decreased as a result of NH_3 interacting with polymeric vanadyl species. Following this, introduction of a NO + O_2 atmosphere to the system caused the intensity of the 900 cm^{-1} band to increase, suggesting that NH_3 interacting with polymeric vanadyl species reacted with NO + O_2, allowing for more polymeric vanadyl species to be detected. Although our previous study[22] showed that NH_3 preferentially adsorbs on Ti surface sites on V/Ti catalysts, V sites can also act as acid sites capable of adsorbing NH_3 molecules. The intensities of the band associated with polymeric species (900 cm^{-1}) and those for crystalline V_2O_5 decreased and increased, respectively, with increasing NH_3 + NO + O_2 exposure before stabilizing, indicating that some of the polymeric vanadyl species reversibly transformed into crystalline V_2O_5. When only NO + O_2 was present (i.e., shutting off NH_3), the intensity of the band at 900 cm^{-1} gradually weakened with increasing exposure time, while the bands at 993 and 1030 cm^{-1} both gradually strengthened. Further oxidation of the sample at 250 °C (under O_2/Ar) again resulted in the appearance of crystalline V_2O_5 and a decrease in polymeric species. Conversion of crystalline V_2O_5 to polymeric species was partly reversible, although it did not recover its original state. After the reaction progressed, crystalline V_2O_5 and monomeric and polymeric vanadyl species were all present on the catalyst surface.

Figure 5 schematically shows the structural transformation of crystalline V_2O_5 on V/Ti-850 inferred from the experimental results. In the presence of NH_3, crystalline V_2O_5 on V/Ti-850 transformed into a polymeric vanadyl species as a result of the lower formation energy for NH_3 adsorbed on polymeric vanadyl species than that on crystalline V_2O_5. In our previous study,[22] polymeric vanadyl species were found to determine the NH_3-SCR activity at low temperatures. Therefore, the active sites were generated under NH_3 conditions, and V/Ti-850 exhibited excellent catalytic performance for NH_3-SCR at a low temperature. When the sample was exposed to O_2 again, a part of polymeric vanadyl species reverted to crystalline V_2O_5.

It was reported that bulk vanadium oxide catalysts and W-substituted vanadium oxide catalysts show excellent NH_3-SCR activity, even at low temperatures below 150 °C.[38,39] In our work, *in situ* Raman results showed that the presence of NH_3 induces the transformation of crystalline V_2O_5 to polymeric vanadyl species, leading to remarkably enhanced catalytic performance at low temperatures. This illustrates exactly the mechanism for the high activity of the bulk V_2O_5 catalyst.

https://doi.org/10.1021/jacs.1c05354
J. Am. Chem. Soc. 2021, 143, 10454−10461

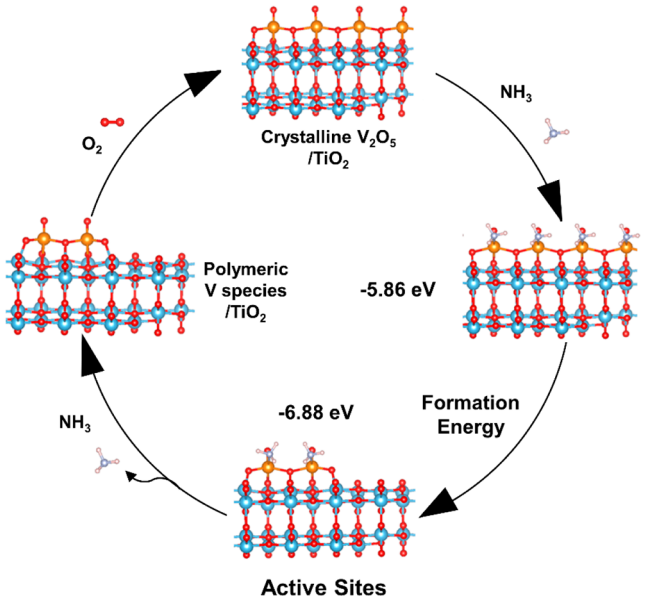

Figure 5. Schematic of the structural transformation of V_2O_5 on the V/Ti-850 catalyst.

However, the tendency of V_2O_5 to spread on TiO_2 might also be influenced by the preparation conditions, including the vanadium loading. Further research into conditions causing the spreading of crystalline V_2O_5 is ongoing.

CONCLUSION

High-temperature (850 °C) calcination of the TiO_2 support in advance of loading with vanadia resulted in a decrease in the specific surface area, an enhancement in anatase crystallinity, and the formation of crystalline V_2O_5 on the surface of the V/Ti-850 catalysts. In addition, the calcined V/Ti-850 catalyst did not have any advantages in terms of redox capability or surface acidity, which were both traditionally considered to be required in the NH_3-SCR of NO_x. However, V/Ti-850 showed significantly higher catalytic activity at low temperatures than untreated V/Ti. For the first time, we find that crystalline V_2O_5 on low-vanadium-loading catalysts can transform to a polymeric vanadyl species under NH_3-SCR reaction conditions, thereby generating active sites, which remarkably enhance the catalytic performance of the vanadia-based catalyst at a low temperature. The active sites generated under reaction conditions played an important role in the NH_3-SCR reaction. This work offers an effective new approach that can guide the preparation of catalysts for commercial applications.

ASSOCIATED CONTENT

Supporting Information

The Supporting Information is available free of charge at https://pubs.acs.org/doi/10.1021/jacs.1c05354.

XRD profiles, NH_3-SCR activity, effect of SO_2 on NO_x conversion, NH_3-TPD results, *in situ* DRIFTS, *in situ* Raman spectra, DFT calculation, and plot of the change in integral area of various Raman peaks (PDF)

AUTHOR INFORMATION

Corresponding Authors

Jian-Feng Li − *State Key Laboratory of Physical Chemistry of Solid Surfaces, Collaborative Innovation Center of Chemistry for Energy Materials (iChEM), College of Chemistry and Chemical Engineering, College of Materials, College of Energy, Xiamen University, Xiamen, Fujian 361005, People's Republic of China;* orcid.org/0000-0003-1598-6856; Email: li@xmu.edu.cn

Hong He − *Center for Excellence in Regional Atmospheric Environment and Key Laboratory of Urban Pollutant Conversion, Institute of Urban Environment, Chinese Academy of Sciences, Xiamen, Fujian 361021, People's Republic of China; State Key Joint Laboratory of Environment Simulation and Pollution Control, Research Center for Eco-Environmental Sciences, Chinese Academy of Sciences, Beijing 100085, People's Republic of China; University of Chinese Academy of Sciences, Beijing 100049, People's Republic of China*; Email: hhe@iue.ac.cn, honghe@rcees.ac.cn

Authors

Zhihua Lian − *Center for Excellence in Regional Atmospheric Environment and Key Laboratory of Urban Pollutant Conversion, Institute of Urban Environment, Chinese Academy of Sciences, Xiamen, Fujian 361021, People's Republic of China;* orcid.org/0000-0002-7413-180X

Jie Wei − *State Key Laboratory of Physical Chemistry of Solid Surfaces, Collaborative Innovation Center of Chemistry for Energy Materials (iChEM), College of Chemistry and Chemical Engineering, College of Materials, College of Energy, Xiamen University, Xiamen, Fujian 361005, People's Republic of China*

Wenpo Shan − *Center for Excellence in Regional Atmospheric Environment and Key Laboratory of Urban Pollutant Conversion, Institute of Urban Environment, Chinese Academy of Sciences, Xiamen, Fujian 361021, People's Republic of China;* orcid.org/0000-0003-2818-5708

Yunbo Yu − *Center for Excellence in Regional Atmospheric Environment and Key Laboratory of Urban Pollutant Conversion, Institute of Urban Environment, Chinese Academy of Sciences, Xiamen, Fujian 361021, People's Republic of China; State Key Joint Laboratory of Environment Simulation and Pollution Control, Research Center for Eco-Environmental Sciences, Chinese Academy of Sciences, Beijing 100085, People's Republic of China; University of Chinese Academy of Sciences, Beijing 100049, People's Republic of China;* orcid.org/0000-0003-2935-0955

Petar M. Radjenovic − *State Key Laboratory of Physical Chemistry of Solid Surfaces, Collaborative Innovation Center of Chemistry for Energy Materials (iChEM), College of Chemistry and Chemical Engineering, College of Materials, College of Energy, Xiamen University, Xiamen, Fujian 361005, People's Republic of China*

Hua Zhang − *State Key Laboratory of Physical Chemistry of Solid Surfaces, Collaborative Innovation Center of Chemistry for Energy Materials (iChEM), College of Chemistry and Chemical Engineering, College of Materials, College of Energy, Xiamen University, Xiamen, Fujian 361005, People's Republic of China;* orcid.org/0000-0001-9588-9030

Guangzhi He − *State Key Joint Laboratory of Environment Simulation and Pollution Control, Research Center for Eco-Environmental Sciences, Chinese Academy of Sciences, Beijing 100085, People's Republic of China;* orcid.org/0000-0003-1770-3522

https://doi.org/10.1021/jacs.1c05354
J. Am. Chem. Soc. 2021, 143, 10454−10461

Fudong Liu − *Department of Civil, Environmental, and Construction Engineering, Catalysis Cluster for Renewable Energy and Chemical Transformations (REACT), NanoScience Technology Center (NSTC), University of Central Florida, Orlando, Florida 32816, United States;* orcid.org/0000-0001-8771-5938

Zhong-Qun Tian − *State Key Laboratory of Physical Chemistry of Solid Surfaces, Collaborative Innovation Center of Chemistry for Energy Materials (iChEM), College of Chemistry and Chemical Engineering, College of Materials, College of Energy, Xiamen University, Xiamen, Fujian 361005, People's Republic of China;* orcid.org/0000-0002-9775-8189

Complete contact information is available at: https://pubs.acs.org/10.1021/jacs.1c05354

Notes

The authors declare no competing financial interest.

■ ACKNOWLEDGMENTS

This work was supported by the National Natural Science Foundation of China (21637005, 21925404, and 51822811) and the Youth Innovation Promotion Association of Chinese Academy of Sciences (2021303 and 2019045).

■ REFERENCES

(1) Ding, K.; Gulec, A.; Johnson, A. M.; Schweitzer, N. M.; Stucky, G. D.; Marks, L. D.; Stair, P. C. Indentification of active sites in CO oxidation and water-gas shift over supported Pt catalysts. *Science* **2015**, *350* (6257), 189−192.

(2) Paolucci, C.; Parekh, A. A.; Khurana, I.; Di Iorio, J. R.; Li, H.; Albarracin Caballero, J. D.; Shih, A. J.; Anggara, T.; Delgass, W. N.; Miller, J. T.; Ribeiro, F. H.; Gounder, R.; Schneider, W. F. Catalysis in a Cage: Condition-Dependent Speciation and Dynamics of Exchanged Cu Cations in SSZ-13 Zeolites. *J. Am. Chem. Soc.* **2016**, *138* (18), 6028−6048.

(3) Malta, G.; Kondrat, S. A.; Freakley, S. J.; Davies, C. J.; Lu, L.; Dawson, S.; Thetford, A.; Gibson, E. K.; Morgan, D. J.; Jones, W.; Wells, P. P.; Johnston, P.; Catlow, C. R. A.; Kiely, C. J.; Hutchings, G. J. Identification of single-site gold catalysis in acetylene hydrochlorination. *Science* **2017**, *355* (6332), 1399−1402.

(4) Marberger, A.; Petrov, A. W.; Steiger, P.; Elsener, M.; Kröcher, O.; Nachtegaal, M.; Ferri, D. Time-resolved copper speciation during selective catalytic reduction of NO on Cu-SSZ-13. *Nat. Catal.* **2018**, *1* (3), 221−227.

(5) Tao, F.; Dag, S.; Wang, L.-W.; Liu, Z.; Butcher, D. R.; Bluhm, H.; Salmeron, M.; Somorjai, G. A. Break-Up of Stepped Platinum Catalyst Surfaces by High CO Coverage. *Science* **2010**, *327*, 850−853.

(6) Yoshida, H.; Kuwauchi, Y.; Jinschek, J. R.; Sun, K.; Tanaka, S.; Kohyama, M.; Shimada, S.; Haruta, M.; Takeda, S. Visualizing Gas Molecules Interacting with Supported Nanoparticulate Catalysts at Reaction Conditions. *Science* **2012**, *335*, 317−319.

(7) Tao, F.; Grass, M. E.; Zhang, Y.; Butcher, D. R.; Renzas, J. R.; Liu, Z.; Chung, J. Y.; Mun, B. S.; Salmeron, M.; Somorjai, G. A. Reaction-Driven Restructuring of Rh-Pd and Pt-Pd Core-Shell Nanoparticles. *Science* **2008**, *322*, 932−934.

(8) Paolucci, C.; Khurana, I.; Parekh, A. A.; Li, S.; Shih, A. J.; Li, H.; Di Iorio, J. R.; Albarracin-Caballero, J. D.; Yezerets, A.; Miller, J. T.; Delgass, W. N.; Ribeiro, F. H.; Schneider, W. F.; Gounder, R. Dynamic multinuclear sites formed by mobilized copper ions in NO_x selective catalytic reduction. *Science* **2017**, *357* (6354), 898−903.

(9) Wachs, I. E. Catalysis science of supported vanadium oxide catalysts. *Dalton Trans* **2013**, *42* (33), 11762−9.

(10) Artiglia, L.; Agnoli, S.; Granozzi, G. Vanadium oxide nanostructures on another oxide: The viewpoint from model catalysts studies. *Coord. Chem. Rev.* **2015**, *301*−*302*, 106−122.

(11) Song, I.; Youn, S.; Lee, H.; Lee, S. G.; Cho, S. J.; Kim, D. H. Effects of microporous TiO_2 support on the catalytic and structural properties of V_2O_5/microporous TiO_2 for the selective catalytic reduction of NO by NH_3. *Appl. Catal., B* **2017**, *210*, 421−431.

(12) Marberger, A.; Ferri, D.; Elsener, M.; Sagar, A.; Artner, C.; Schermanz, K.; Krocher, O. Relationship between structures and activities of supported metal vanadates for the selective catalytic reduction of NO by NH_3. *Appl. Catal., B* **2017**, *218*, 731−742.

(13) Zhang, D.; Yang, R. T. NH_3-SCR of NO over one-pot Cu-SAPO-34 catalyst: Performance enhancement by doping Fe and MnCe and insight into N_2O formation. *Appl. Catal., A* **2017**, *543*, 247−256.

(14) Zhu, M.; Lai, J. K.; Tumuluri, U.; Wu, Z.; Wachs, I. E. Nature of Active Sites and Surface Intermediates during SCR of NO with NH_3 by Supported V_2O_5-WO_3/TiO_2 Catalysts. *J. Am. Chem. Soc.* **2017**, *139* (44), 15624−15627.

(15) Bukowski, A.; Schill, L.; Nielsen, D.; Mossin, S.; Riisager, A.; Albert, J. NH_3-SCR of NO with novel active, supported vanadium-containing Keggin-type heteropolyacid catalysts. *React. Chem. Eng.* **2020**, *5* (5), 935−948.

(16) Putluru, S. S. R.; Jensen, A. D.; Riisager, A.; Fehrmann, R. Heteropoly acid promoted V_2O_5/TiO_2 catalysts for NO abatement with ammonia in alkali containing flue gases. *Catal. Sci. Technol.* **2011**, *1* (4), 631−637.

(17) Putluru, S. S. R.; Schill, L.; Gardini, D.; Mossin, S.; Wagner, J. B.; Jensen, A. D.; Fehrmann, R. Superior $DeNO_x$ activity of V_2O_5-WO_3/TiO_2 catalysts prepared by deposition-precipitation method. *J. Mater. Sci.* **2014**, *49* (7), 2705−2713.

(18) Tao, M.; Ishikawa, S.; Murayama, T.; Inomata, Y.; Kamiyama, A.; Ueda, W. Synthesis of Zeolitic Mo-Doped Vanadotungstates and Their Catalytic Activity for Low-Temperature NH_3-SCR. *Inorg. Chem.* **2021**, *60* (7), 5081−5086.

(19) Went, G. T.; Leu, L.-J.; Rosin, R. R.; Bell, A. T. The effect of structure on the catalytic activity and selectivity of V_2O_5/TiO_2 for the reduction of NO by NH_3. *J. Catal.* **1992**, *134*, 492−505.

(20) Went, G. T.; Oyama, S. T.; Bell, A. T. Laser Raman Spcetroscopy of Supported Vanadium Oxide Catalysts. *J. Phys. Chem.* **1990**, *94*, 4240−4246.

(21) Choo, S. T.; Lee, Y. G.; Nam, I.-S.; Ham, S.-W.; Lee, J.-B. Characteristics of V_2O_5 supported on sulfated TiO_2 for selective catalytic reduction of NO by NH_3. *Appl. Catal., A* **2000**, *200*, 177−188.

(22) He, G.; Lian, Z.; Yu, Y.; Yang, Y.; Liu, K.; Shi, X.; Yan, Z.; Shan, W.; He, H. Polymeric vanadyl species determine the low-temperature activity of V-based catalysts for the SCR of NO_x with NH_3. *Sci. Adv.* **2018**, *4*, eaau4637.

(23) Lian, Z.; Shan, W.; Zhang, Y.; Wang, M.; He, H. Morphology-Dependent Catalytic Performance of NbO_x/CeO_2 Catalysts for Selective Catalytic Reduction of NO_x with NH_3. *Ind. Eng. Chem. Res.* **2018**, *57* (38), 12736−12741.

(24) Perdew, J. P.; Burke, K.; Ernzerhof, M. Generalized gradient approximation made simple. *Phys. Rev. Lett.* **1996**, *77* (18), 3865−3868.

(25) Kresse, G.; Furthmuller, J. Efficient iterative schemes for ab initio total-energy calculations using a plane-wave basis set. *Phys. Rev. B: Condens. Matter Mater. Phys.* **1996**, *54* (16), 11169−11186.

(26) Kresse, G.; Joubert, D. From ultrasoft pseudopotentials to the projector augmented-wave method. *Phys. Rev. B: Condens. Matter Mater. Phys.* **1999**, *59* (3), 1758−1775.

(27) Lutfalla, S.; Shapovalov, V.; Bell, A. T. Calibration of the DFT/GGA plus U Method for Determination of Reduction Energies for Transition and Rare Earth Metal Oxides of Ti, V, Mo, and Ce. *J. Chem. Theory Comput.* **2011**, *7* (7), 2218−2223.

(28) Besselmann, S.; Loffler, E.; Muhler, M. On the role of monomeric vanadyl species in toluene adsorption and oxidation on V_2O_5/TiO_2 catalysts: A Raman and in situ DRIFTS study. *J. Mol. Catal. A: Chem.* **2000**, *162*, 401−411.

(29) Due-Hansen, J.; Boghosian, S.; Kustov, A.; Fristrup, P.; Tsilomelekis, G.; Stahl, K.; Christensen, C. H.; Fehrmann, R.

Vanadia-based SCR catalysts supported on tungstated and sulfated zirconia: Influence of doping with potassium. *J. Catal.* **2007**, *251* (2), 459−473.
(30) Topsoe, N. Y. Mechanism of the selective catalytic reduction of nitric oxide by ammonia elucidated by in situ online Fourier Transform Infrared spectroscopy. *Science* **1994**, *265* (5176), 1217−1219.
(31) Bond, G. C.; Flamerz, S.; Shukri, R. Structure and Reactivity of Transition-metal Oxide Monolayers. *Faraday Discuss. Chem. Soc.* **1989**, *87*, 65−77.
(32) Nie, A.; Yang, H.; Li, Q.; Fan, X.; Qiu, F.; Zhang, X. Catalytic Oxidation of Chlorobenzene over V_2O_5/TiO_2−Carbon Nanotubes Composites. *Ind. Eng. Chem. Res.* **2011**, *50* (17), 9944−9948.
(33) Marberger, A.; Ferri, D.; Elsener, M.; Krocher, O. The Significance of Lewis Acid Sites for the Selective Catalytic Reduction of Nitric Oxide on Vanadium-Based Catalysts. *Angew. Chem., Int. Ed.* **2016**, *55* (39), 11989−11994.
(34) Mu, J.; Li, X.; Sun, W.; Fan, S.; Wang, X.; Wang, L.; Qin, M.; Gan, G.; Yin, Z.; Zhang, D. Inductive Effect Boosting Catalytic Performance of Advanced $Fe_{1-x}V_xO_\delta$ Catalysts in Low-Temperature NH_3 Selective Catalytic Reduction: Insight into the Structure, Interaction, and Mechanisms. *ACS Catal.* **2018**, *8* (8), 6760−6774.
(35) Kwon, D. W.; Park, K. H.; Ha, H. P.; Hong, S. C. The role of molybdenum on the enhanced performance and SO_2 resistance of V/Mo-Ti catalysts for NH_3-SCR. *Appl. Surf. Sci.* **2019**, *481*, 1167−1177.
(36) Haber, J.; Machej, T.; Serwicka, E. M.; Wachs, I. E. Mechanism of surface spreading in vanadia-titania system. *Catal. Lett.* **1995**, *32*, 101−115.
(37) Wang, C.-B.; Cai, Y.; Wachs, I. E. Reaction-induced spreading of metal oxides onto surfaces of oxide supports during alcohol oxidation: Phenomenon, nature, and mechanisms. *Langmuir* **1999**, *15* (4), 1223−1235.
(38) Inomata, Y.; Hata, S.; Mino, M.; Kiyonaga, E.; Morita, K.; Hikino, K.; Yoshida, K.; Kubota, H.; Toyao, T.; Shimizu, K.-i.; Haruta, M.; Murayama, T. Bulk Vanadium Oxide versus Conventional V_2O_5/TiO_2: NH_3-SCR Catalysts Working at a Low Temperature Below 150 °C. *ACS Catal.* **2019**, *9* (10), 9327−9331.
(39) Inomata, Y.; Kubota, H.; Hata, S.; Kiyonaga, E.; Morita, K.; Yoshida, K.; Sakaguchi, N.; Toyao, T.; Shimizu, K.-i.; Ishikawa, S.; Ueda, W.; Haruta, M.; Murayama, T. Bulk tungsten-substituted vanadium oxide for low-temperature NO_x removal in the presence of water. *Nat. Commun.* **2021**, *12* (1), 557.

https://doi.org/10.1021/jacs.1c05354
J. Am. Chem. Soc. 2021, 143, 10454−10461